Project Number: VVY-1401

Modeling-Based Optimization of Thermal Processing in Microwave Fixation

A Major Qualifying Project

Submitted to Faculty

of the

WORCESTER POLYTECHNIC INSTITUTE

In partial fulfillment of the requirements for the

Degree of Bachelor of Science

by

Ethan M. Moon

April 30, 2015

Advised by:

Professor Vadim V. Yakovlev

Abstract

Principles of homogenization of thermal processing in microwave fixation are described along with a corresponding modeling-based optimization procedure. An innovative microwave fixation system is computationally analyzed. Two geometric parameters as well as complex permittivity of a dielectric insert are identified as design variables of the optimization problem. Performing an illustrative optimization, the procedure outputs the parameters of the system with the relative standard deviation (served as a uniformity metric) of dissipated power reduced by 5 times.

Acknowledgement

I would like to thank:

- Dr. Vadim V. Yakovlev, Worcester Polytechnic Institute, Worcester, MA – for his constant guidance and seemingly unending patience;
- Dr. Ethan K. Murphy, formerly Applied Mathematics, Inc., Gales Ferry, CT, currently Thayler School of Engineering, Dartmouth College, Hanover, NH – for his help with numerous implementation issues as well as his valuable insight through the course of the project;
- Dr. Charles Scouten, Neuroscience Tools, Downers Grove, IL – for his help and guidance in solving the biological issues related to the project;
- John F. Gerling, Gerling Applied Engineering, Inc., Modesto, CA – for his help designing an effective model for simulation purposes.
- Christine Petzold, Assumption College, Worcester, MA – for her help developing my writing skills into something remotely presentable.

Table of Contents

List of Figures and Tables

1. Introduction

1.1 Background

Post-sacrifice chemical analysis of brain chemistry is a critical and challenging part of neurological studies of numerous disorders, such as Parkinson's disease, schizophrenia, bipolar disorder, traumatic brain injury, Alzheimer's, multiple sclerosis, epilepsy, stroke, and so on [1-4]. In 2004, 13% of the global health burden was caused by neurological disorders [5]. The majority of people diagnosed with these disorders are not functional in society and cannot live without consistent medication or management by others.

Diagnosis is usually based on analyzing the behavioral symptoms of the patient, with the root cause rarely known or understood. Developing effective means of testing treatments on animals for humanlike disorders is therefore an exceptional goal of neurological research. Using animal models to investigate behavioral disorders work as a parallel to humanlike disorders because functionally, the processes in the brain are similar to that of a human. The mammalian brain performs most of its processes through chemical means, so the chemical transmission mechanism provides an accessible point of entry where a drug may act to enhance, reduce, or block particular functions of neurons.

Abnormal chemistry of the brain is an important cause in many brain disorders. Chemical levels in the brain are tightly regulated within narrow limits by enzymes, which are proteins that catalyze brain chemical actions. There is a balance between synthesis and breakdown of any brain molecule. Typically, one side of the reaction requires energy to perform the catalyzing, the other side does not. Immediately upon disruption of oxygen flow, energy use in the brain stops. The enzymes present that do not use energy continue to catalyze reactions, either synthesizing proteins or breaking them down. Enzymes that require oxygen to work are still present, but promptly stop working. As a result, within seconds, most chemicals in the brain have either increased or decreased in quantity to well outside the physiological range.

This poses a significant problem for the researchers aiming to identify brain chemistry that is abnormal. Upon removal of tissue for a test to begin, levels of all chemicals within the tissue will change dramatically. Early on, various methods of freezing the brain were tried to stop this process. However, it may take up to 90 seconds for the interior of the animal's head to freeze, which is much too slow for lifelike chemistry. Freezing keeps the enzymes present and undamaged; as a result, if the brain tissue is thawed at any point during its analysis, the proportion of the chemicals is greatly altered from the lifelike state.

Fixation, an alternative technique proposed in [6], suggests stopping all enzyme activity in the brain immediately and permanently by heating rather than freezing. It was determined that a very fast heating of the brain tissue up to the level of 80-90^{o}C would achieve the goal of locking the chemical state of the brain.

When designing a practical equipment for this process, microwave systems became a natural choice because they allow for variability in the power setting as well as duration of heating. After the pioneering paper [6], the technology of microwave fixation was identified as a highly promising (if not the only possible) way to lock the chemical state of the brain for post-sacrifice chemical analysis. In theory, the higher the power is set, the faster the process of fixation can be performed. However, designing efficient microwave systems capable of rigid contol over the process is a very difficult task due to the fact that microwave thermal processing is intrinsically non-homogeneous [7], whereas the apparatuses for microwave fixation must provide the required level of temperature uniformity (80-90^{o}C) precisely in the

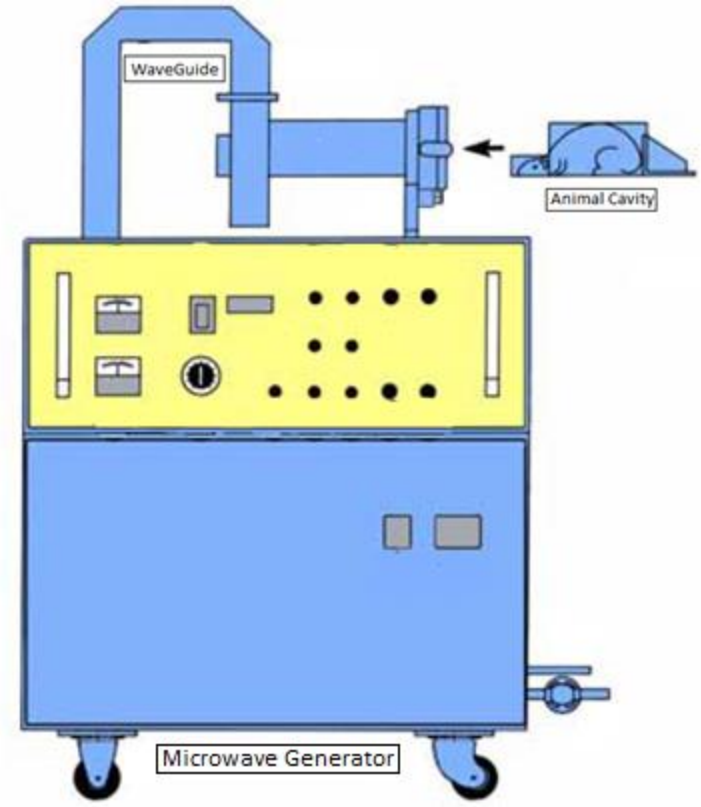

Figure 1.1. Diagram of the TMW-4012C Muromachi system.

brain tissue. So far, there are very few microave systems on the market available for study of brain chemistry. Therefore, the development of new efficient applicators for neurolocial studies is in high demand.

1.2 Microwave Systems

Commercially available applicators consist of a microwave generator and an applicator where fast microwave heating of brain tissue takes place. The applicator is typically built on a single-mode rectangular waveguide. An animal is positioned with the body held in a cavity extending out of the waveguide and the head is inserted into it. Two of the most popular microwave fixation applicators (from Muromachi Kikai

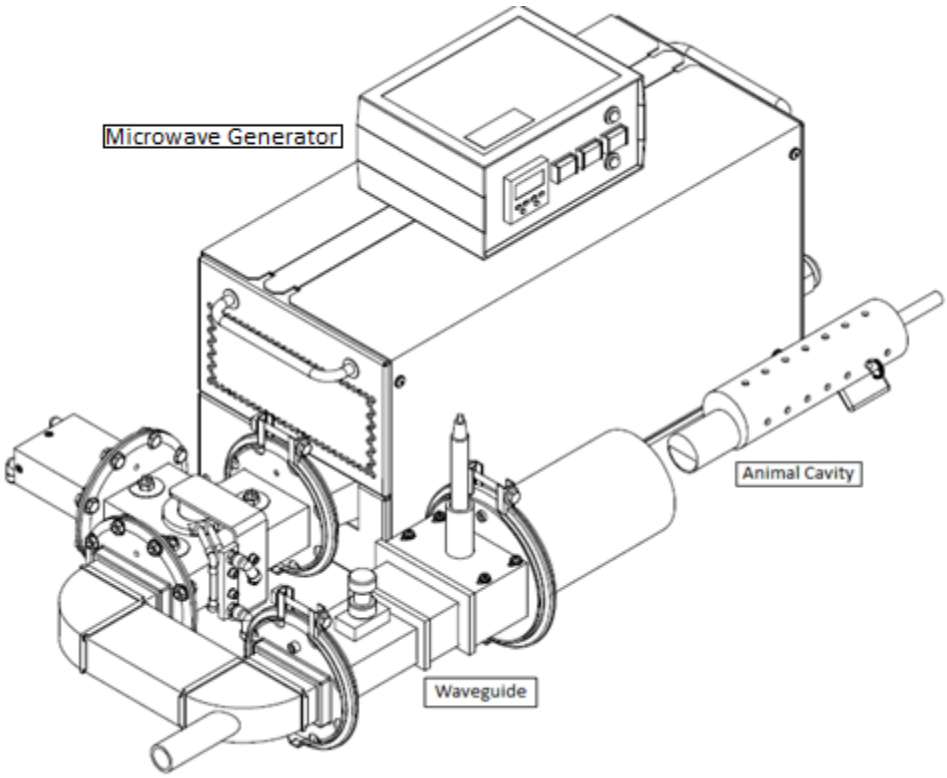

Figure 1.2. Diagram of the GA5013 GAE's system.

Co., LTD, Japan [8] and Gerling Applied Engineering, Inc. (GAE), CA [9]) are briefly described below. It appears that both devices use rather inefficient technical solutions and hardly control the temperature field in the brain tissue, whereas homogeneous thermal treatment is a strict requirement.

Muromachi System. The TMW-4012C Muromachi microwave fixation device, shown in Figure 1.1, is currently considered the leader on the market. In an attempt to facilitate the creation of homogenous thermal processing, the device utilizes a water jacket surrounding the animal's head. The TWM-4012C system has a variable power output from 3 kW to 10 kW. This high level of microwave power is necessary to heat brain tissue, which is characterized by a low loss factor (compared to water) and therefore heating of the animal's head occurs at a significantly lower rate.

Gerling System. The GA5013 Gerling microwave fixation device, shown in Figure 1.2, has a variable power setting between 2 kW and 4 kW. The system does not utilize water to redistribute the electric field around the animal's head like the Muromachi device, but instead relies solely on the central placement

of the animal's head within the waveguide. Therefore, the level of microwave power in the Gerling system is lower, however, the absence of the means aiming to homogenize the heating of the brain tissue provides no notable benefits for this device compared to Muromachi's.

1.3 Project Objectives

Analysis of the described equipment suggests that existing systems for microwave fixation are operationally cumbersome and energy inefficient. Therefore, the objective of this project was to develop an optimization procedure to assist in the computer-aided design (CAD) of new efficient systems for microwave fixation.

We report the results of an initial exploration of an alternative microwave system design, featuring a solid dielectric insert. The insert's shape and complex permittivity are determined for a given brain's material parameters and geometry so that the dissipated power distribution in the animal's head is as homogeneous as possible. The corresponding optimization problem is formulated and solved with the use of a computational procedure using numerical data generated by a 3D model representing the microwave system.

2. Methodology

2.1 Advanced Fictional System and Its Computer Model

At the first step of the project, we introduce a design of a fictional microwave applicator, whose structure is conceptually similar to the Gerling system, but relies on a solid dielectric insert to achieve homogeneous thermal treatment. The proposed applicator consists of a section of a single-mode rectangular waveguide, centrally connected with a cylindrical cavity of a diameter exceeding the wide wall of the waveguide. The animal is positioned so that the body is in the cavity, and the head in the waveguide. The entirety of the head is surrounded by a rectangular dielectric insert, with a cone that covers the side facing the input of the applicator to improve the matching of the loaded system with the microwave generator. This proposed design of the applicator is illustrated by Figures 2.1 and 2.2.

The entire fictional system has been reproduced in a 3D fully parameterized model built for the full-wave conformal Finite-Difference Time-Domain (FDTD) simulator *QuickWave 2014* [10]. In the model, the animal's body and head are approximated by a cylinder and a truncated cone, and we utilize the value of complex permittivity for a mouse brain (gray tissue) as $\varepsilon_m = 46.9 - j7.2$ [11] at 2.45 GHz. To ensure high solution accuracy, the scenario in the model is discretized with a non-uniform mesh (with max cell

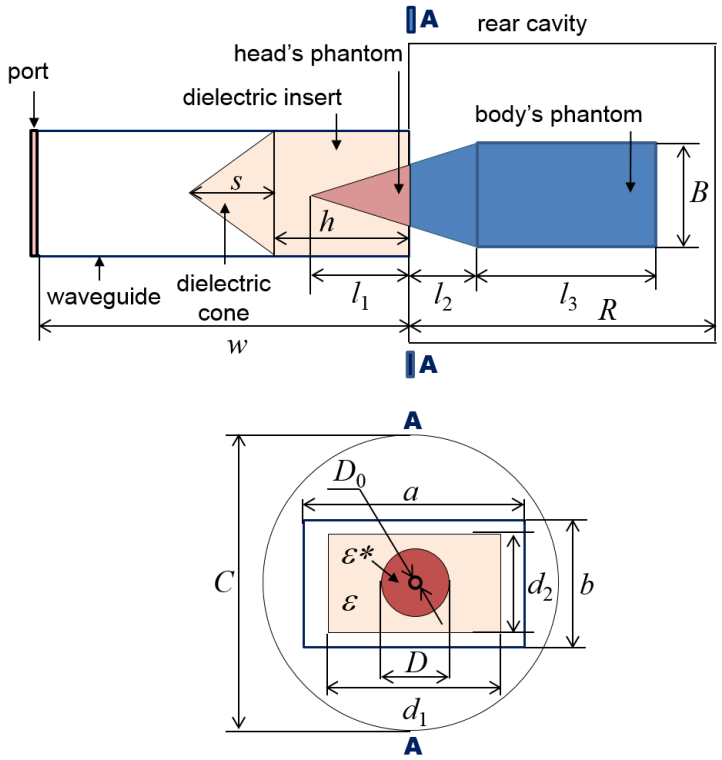

Figure 2.1. Sketch of the considered fictional microwave system.

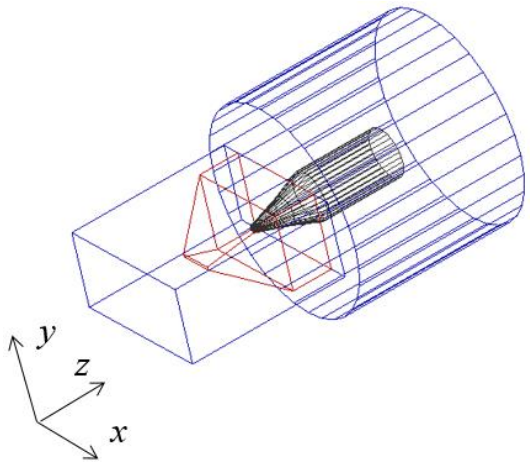

Figure 2.2. 3D view of the microwave system introduced in detail in Figure 2.1.

sizes of 5 mm in air and 1.5 mm in the insert and in the animal), and thus the model contains roughly 560,000 cells. The details of discretization of the system are shown in Appendix A.1.

The process of microwave fixation is very quick (less than 1 s); this implies that the time for alterations of the microwave heating pattern due to heat diffusion is negligible. Therefore, our computational task can be reduced to finding a numerical solution of the electromagnetic problem; more specifically, to determination of distributions of dissipated power (which subsequently could be optimized).

2.2 Dissipated Power Distribution – Computational Tests

In order to determine the most influential parameters and identify the design variables of the forthcoming optimization, systematic computational experiments were performed for various geometrical and material parameters of the system.

From the preliminary simulation, it was found that the structure of the electric field and corresponding dissipated power inside the head's phantom did not notably change with variation of some parameters of the system (e.g., geometrical parameters of the rear cavity *R* and *C*). Other parameters, like the length of the dielectric cone *s*, may affect the field in the insert, but those characteristics should be considered in terms of the reflections from the system and should not be arbitrarily changed to control the field distribution. Four parameters of the dielectric insert were identified as being particularly influential on the distribution of the field inside the head's phantom:

- Width d_1 (mm)
- Height d_2 (mm)
- Dielectric constant ε'
- The loss factor ε'' (or its derivative, electric conductivity σ(S/m))

For these parameters (forming a vector in a design space), ten sets of computational tests have been performed as described in Table 2.1. In each set, three parameters were kept constant, whereas the remaining one varied over a wide interval; the output of each simulation included the electric field in the entire applicator and dissipated power inside the material

Table 2.1. Series of Initial Computational Tests

Set	Constant Parameters			Variable Parameter	Range of Variation
1	d_1 = 80 mm	d_2 = 55 mm	$0.026 \le \sigma \le 0.11$ S/m ($0.184 \le \varepsilon'' \le 0.808$)	ε'	6.7, 1.5, 25, 35, 45
2	d_1 = 80 mm	d_2 = 55 mm	$\varepsilon' = 6.7$	σ (ε'')	0.026, 0.25, 0.5, 0.75, 1.0 S/m (0.19, 1.84, 3.67, 5.51, 7.34)
3	d_2 = 55 mm	$\varepsilon' = 6.69$	$\sigma = 0.026$ S/m ($\varepsilon'' = 0.184$)	d_1	80, 70, 60, 50, 40, 30 mm
4	d_2 = 55 mm	$\varepsilon' = 25$	$\sigma = 0.07$ S/m ($\varepsilon'' = 0.514$)	d_1	80, 70, 60, 50, 40, 30 mm
5	d_2 = 55 mm	$\varepsilon' = 46$	$\sigma = 0.11$ S/m ($\varepsilon'' = 0.808$)	d_1	80, 70, 60, 50, 40, 30 mm
6	d_2 = 55 mm	$\varepsilon' = 63$	$\sigma = 0.75$ S/m ($\varepsilon'' = 5.51$)	d_1	80, 70, 60, 50, 40, 30 mm
7	d_2 = 55 mm	$\varepsilon' = 78$	$\sigma = 1.19$ S/m ($\varepsilon'' = 8.74$)	d_1	80, 70, 60, 50, 40, 30 mm
8	d_1 = 40 mm	$\varepsilon' = 25$	$\sigma = 0.07$ S/m ($\varepsilon'' = 0.514$)	d_2	55, 45, 35 mm
9	d_1 = 40 mm	$\varepsilon' = 63$	$\sigma = 0.75$ S/m ($\varepsilon'' = 5.51$)	d_2	55, 45, 35 mm
10	d_1 = 40 mm	$\varepsilon' = 78$	$\sigma = 1.19$ S/m ($\varepsilon'' = 8.74$)	d_2	55, 45, 35 mm

(i.e., the dielectric insert, the body's phantom and the head's phantom). The structure of the field and distribution of the dissipated power dramatically vary, even with small variations of each of these parameters. This series of computational tests is not representative of the entire system because variation only takes place in the considered intervals. However, comparative analysis of the results allows us to make some general conclusions about the roles played by these parameters in the system and choose the bounds specifying the space in the subsequent optimization.

Tables 2.2-2.4 contain a selection of 2D visualizations of volumetric heating patterns in the enclosed dielectric structure formed by the body's phantom and the insert containing the head's phantom. The region in which a significant level of uniformity of dissipated power is required is the small conical volume inside the insert that reproduces the animal's head (shown in pink in Figure 2.1). It is seen from the patterns in the tables that the region of interest is heated in a highly non-uniform fashion. The pattern corresponding to $\varepsilon' = 6.7$, and $\sigma = 1.0$ S/m should be considered an exception because the magnitude of dissipated power in the head's phantom is very small with respect to the peak values outside of this region.

Table 2.2. Patterns of Dissipated Power in the XZ-Plane: Variation of ε' and σ

Dielectric constant (ε')	**25**	**35**	**45**
Constant parameters: σ = 0.09 (S/m), d_1 = 80 mm, d_2 = 55 mm	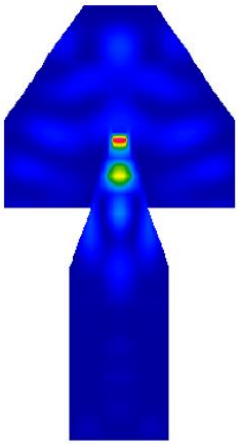	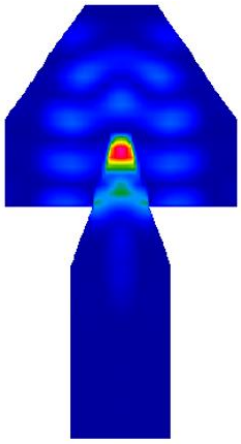	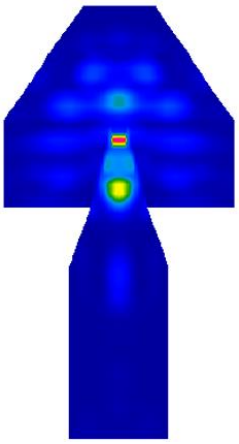
Conductivity (σ)	**0.026**	**0.5**	**1.0**
Constant parameters: ε' = 6.7, d_1 = 80 mm, d_2 = 55 mm	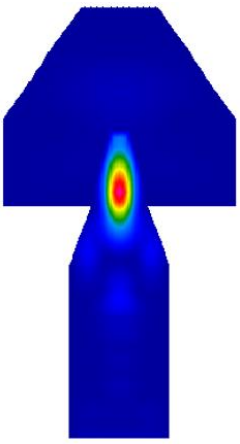	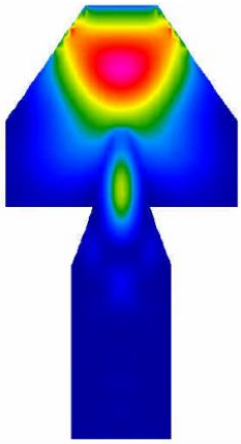	

This strong difference in the level of dissipated power would be a significant disadvantage of the system for microwave fixation in terms of energy efficiency.

2.3 Metric of Uniformity

To properly characterize the uniformity of dissipated power within the animal's head, an appropriate metric needs to be determined. As indicated in Section 2.1, dissipated power is considered the only factor responsible for forming microwave-induced temperature fields. However, the review of the metrics used in

Table 2.3. Patterns of Dissipated Power in the XZ-Plane: Variation of d_1

Dimension (d_1)	**40**	**60**	**80**
Constant parameters: $\varepsilon' = 25$, $\sigma = 0.07$ (S/m), $d_2 = 55$ mm	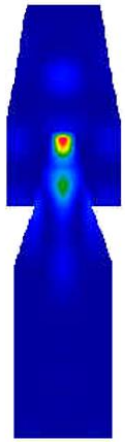	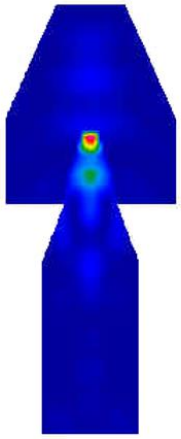	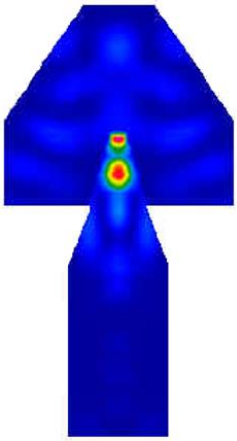
Dimension (d_1)	**40**	**60**	**80**
Constant parameters: $\varepsilon' = 63$, $\sigma = 0.75$ (S/m), $d_2 = 55$ mm	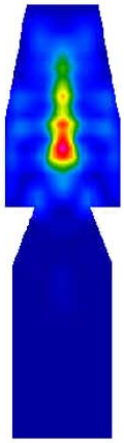	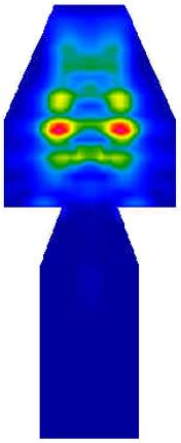	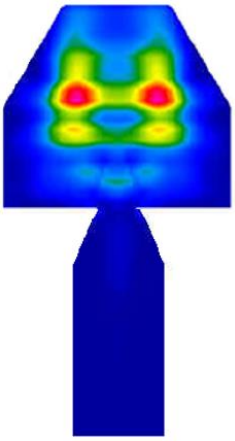

the literature on modeling and optimization of microwave heating processes and systems [7] shows that, currently, there is no commonly accepted criterion for measuring the uniformity of the temperature field.

We therefore propose calculating the relative standard deviation (*RSD*) of the values of dissipated power within the FDTD cells located in the head's phantom:

$$RSD = (STD/AVG)100\ (\%),$$

where *STD* is the standard deviation of data set, and *AVG* is the mean of the data set. Low *RSD* indicates

Table 2.4. Patterns of Dissipated Power in the XZ-Plane: Variation of d_2

Dimension (d_2)	**35**	**45**	**55**
Constant parameters: $\varepsilon' = 25$, $\sigma = 0.07$ (S/m), $d_1 = 40$ mm		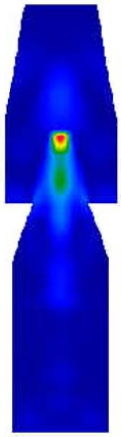	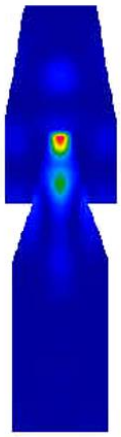
Dimension (d_2)	**35**	**45**	**55**
Constant parameters: $\varepsilon' = 25$, $\sigma = 0.75$ (S/m), $d_1 = 40$ mm	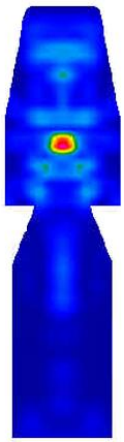		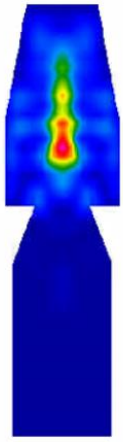

that the data set has little variation, meaning that the pattern of dissipated power is relatively uniformly distributed; large values of *RSD* (including those over 100%) represent highly non-uniform distributions.

2.4 Optimization Procedure

The optimization procedure developed in this project is outlined in Figure 2.3. It is a four-step process, with the first three steps concerned with setting up the problem before it is passed to an optimizer. Step 1 requires the determination of several design variables *N* as well as the physical limitations the device puts on the

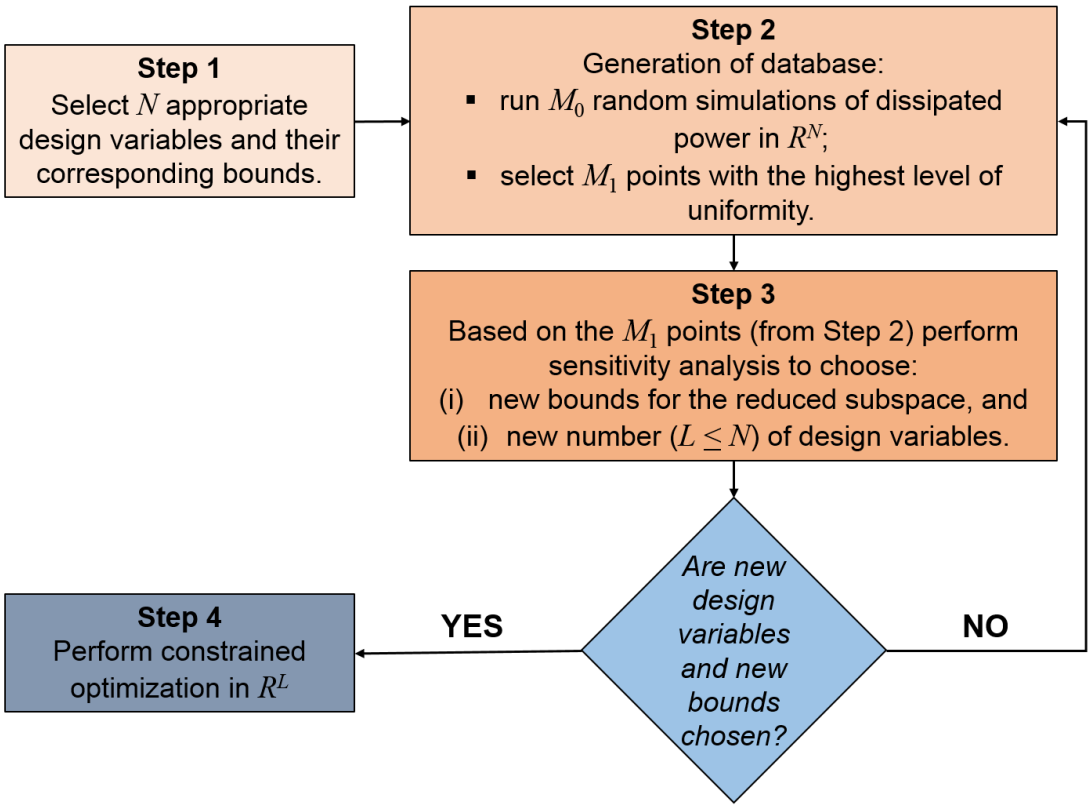

Figure 2.3. Flow-chart of the developed optimization procedure.

ranges of the chosen design variables. These limitations will help choose the lower and upper bounds for the design variables. At Step 2, a comprehensive database containing M_0 points is generated from randomly selected vectors within the design space. For each of these points, an FDTD solution (including the field of dissipated power) is generated and analyzed to determine *RSD*. With a fully analyzed database, M_1 vectors are chosen with the highest levels of uniformity. At Step 3, a sensitivity analysis is performed with the M_1 points as its basis. This is done by variation over the different components of the vector, while all others are kept constant. The purpose of this analysis is to possibly reduce the number of design variables (down to L) and the intervals of their variation. At Step 4, an optimization is performed utilizing L design variables with the bounds of variations determined at Step 3. The technique of this optimization is outlined in the next sub-section.

2.5 Constrained Optimization

Step 4 of the described optimization procedure is the stage at which the problem is actually formulated and solved as a constrained optimization problem. This problem can be described as:

$$\min_{x} f(x) \text{ such that } \begin{cases} c(x) \leq 0 \\ ceq(x) = 0 \\ A \cdot x \leq b \\ Aeq \cdot x = beq \\ lb \leq x \leq ub. \end{cases}$$

where $f(x)$ is the objective function, $c(x)$ and $ceq(x)$ are nonlinear inequality and equality constraints of design variables x; A and Aeq are the linear inequality and equality constraints on the design variables x. When evaluated, A and Aeq must be less than or equal to b or must be equal to beq respectively; lb and ub are the upper and lower bounds for the design variables x.

The key difficulty in the formulation of the optimization problem here comes from the fact that we deal with numerical values, and therefore there is no analytical expression for the objective function. This means that the objective function for each set of the design variables must be calculated explicitly. Also, the step direction during the optimization cannot be calculated using traditional methods relying on computation of the derivative of $f(x)$.

To overcome those difficulties, our choice was to implement an active set algorithm which utilized Sequential Quadratic Programming. The principal idea of this technique lies in formulation of a Quadratic Programming (QP) sub-problem based on a quadratic approximation of the Lagrangian function. This QP sub-problem can be formulated because the Hessian is approximated with each new solution using a quasi-Newton method. This eliminates the need for an analytical objective function. Moreover, once the QP problem is solved, the solution represents the search direction to be used in a standard search procedure to determine the step length. The determined incumbent solution is used to approximate the next Hessian.

The optimization procedure described above was implemented using MATLAB. *QW Editor* and *QW Simulator*, the key modules of *QuickWave 2014*, are called directly from MATLAB command line in an automated regime. The constrained optimization problem at Step 4 is solved with `fmincon` function in the MATLAB Optimization Toolbox.

3. Results

3.1 Illustrative Optimization

The optimization procedure described in Sections 2.4-2.5 has been implemented in MATLAB. To illustrate its functionality, the code was then tested with the model presented in Section 2.1 in order to find optimal parameters of the dielectric insert.

Beginning with Step 1, we identified four appropriate design variables (N = 4) – the dielectric constant (ε'), conductivity (σ), the width (d_1) and height (d_2) of the dielectric insert with the corresponding bounds of the sub-space defined as

$$46 \leq \varepsilon' \leq 80;\ 0.01 \leq \sigma\,(\text{S/m}) \leq 1.0;\ 30 \leq d_1\ (\text{mm}) \leq 80;\ 50 \leq d_2\ (\text{mm}) \leq 60.$$

With design variables chosen and a sub-space identified, we moved onto Step 2 in the procedure building the database. We set M_0 to 560, and generated random values within each design variables bounds. After generation of the database was completed, its contents were analyzed. It turned out that it contained large variation in the range of *RSD* values with the highest being 135.6 % and the lowest being 27.0 %. Moving forward, we set M_1 = 4 choosing the best four sets of design variables corresponding to highest levels of uniformity. The values presented in Table 3.1 are the points chosen from the database.

Table 3.1. Output of Step 1: Values of the Design Variables for Four Lowest Values of *RSD*

Point #	**407**	**333**	**210**	**119**
ε'	63.3	61.7	59.0	60.3
σ (S/m)	0.1636	0.156	0.335	0.333
d_1 (mm)	60.4	60.5	61.3	60.0
d_2 (mm)	55	55	55	55
RSD (%)	30.4	27.5	29.0	27.0

Table 3.2 Optimization Parameters and Results

Design Variable	$x_1 = \varepsilon'$			$x_2 = \sigma$ (S/m)		
Starting Point #	lb_1	Initial Value	ub_1	lb_2	Initial Value	ub_2
407	57	63.3	68	0.1	0.1636	0.2
333	56	61.7	67	0.1	0.156	0.2
210	55	59	66	0.29	0.335	0.39
119	55	60.3	65	0.29	0.333	0.39

Performing several series of simulations around the points in Table 3.1 revealed that they were an accurate representation of local minima. The sensitivity analysis was performed around each point; Figure 3.1 represents *RSD* as functions of one design variable that were obtained while keeping the other variables constant. These variations were not performed over d_2 because its effect was deemed to be negligible after review of the database generated in Step 2.

The sensitivity analysis performed in Step 3 revealed that d_1 could be removed from consideration in Step 4, defining L as 2. We were also able to reduce the ranges of the design variables to the smaller intervals given in Table 3.2. Having reduced the number of design variables to 2 and sufficiently reducing the ranges of variation, we continued to Step 4, at which stage better solutions for local minima are sought. The paths the optimization technique went through are illustrated in Figure 3.2, which shows level curves in the domain around the starting point in Table 3.1. Black dots in these graphs depict the points at which the optimizer stopped before reaching a minimum. Due to the stopping criteria, the minimum at Figure (a) did not reach the light-blue domain corresponding to the smallest values of *RSD* in the chosen sub-space.

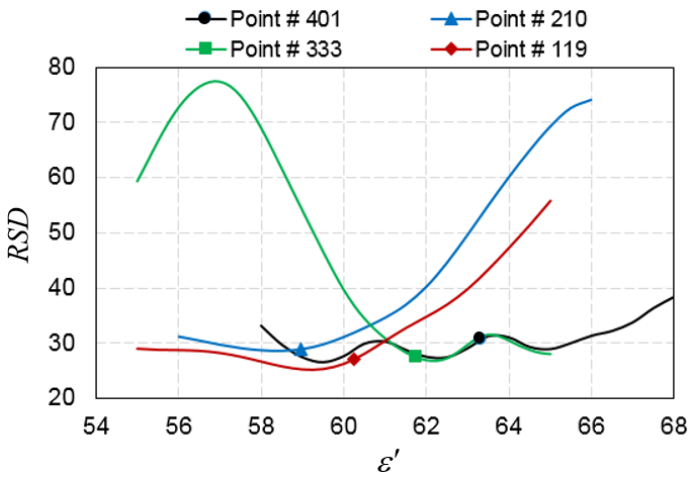

(a)

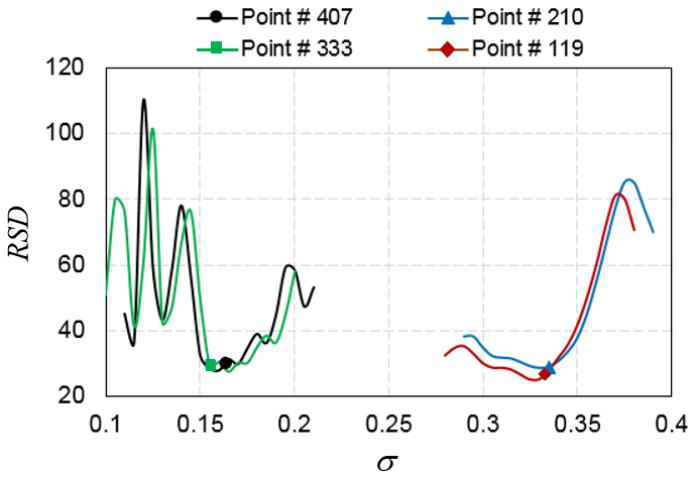

(b)

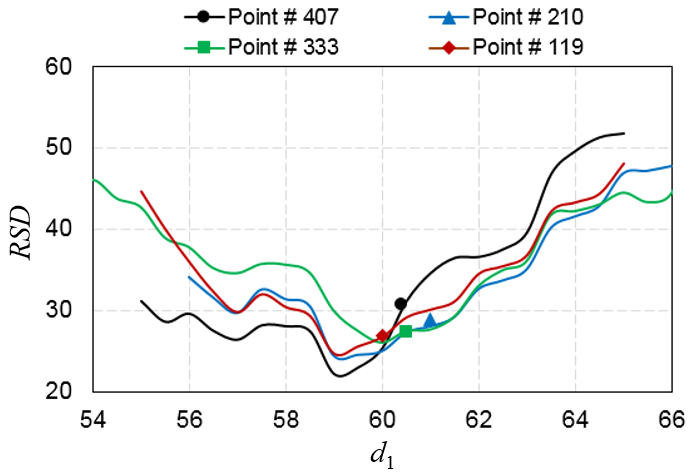

(c)

Figure 3.1. *RSD* as a function of ε' (a), σ (b), and d_1 (c) at four local minima (pts 119, 210, 333, and 407).

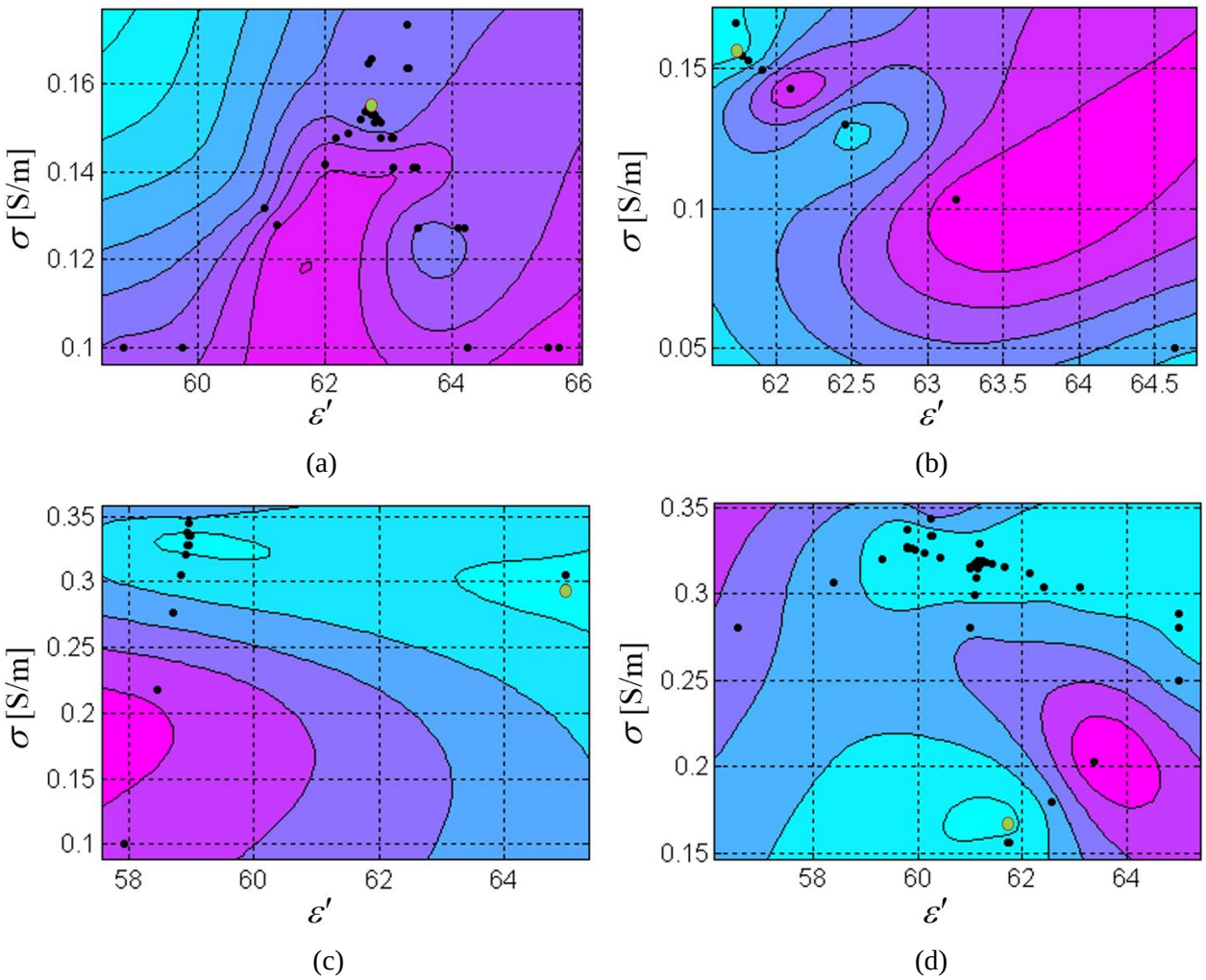

Figure 3.2. Performance of the gradient-type optimization in the sub-space of two design variables (ε' and σ): starting points 407 (a), 333 (b), 210 (c), and 119 (d).

Table 3.3. Output of Step 2: Values of the Design Variables for Four Lowest Values of *RSD*

Minimum Point #	**407+**	**333+**	**210+**	**119+**
ε'	62.7	61.7	65.0	61.7
σ (S/m)	0.155	0.156	0.296	0.166
d_1 (mm)	60.4	60.5	61.3	60.0
d_2 (mm)	55	55	55	55
RSD (%)	26.5	27.5	27.3	23.9

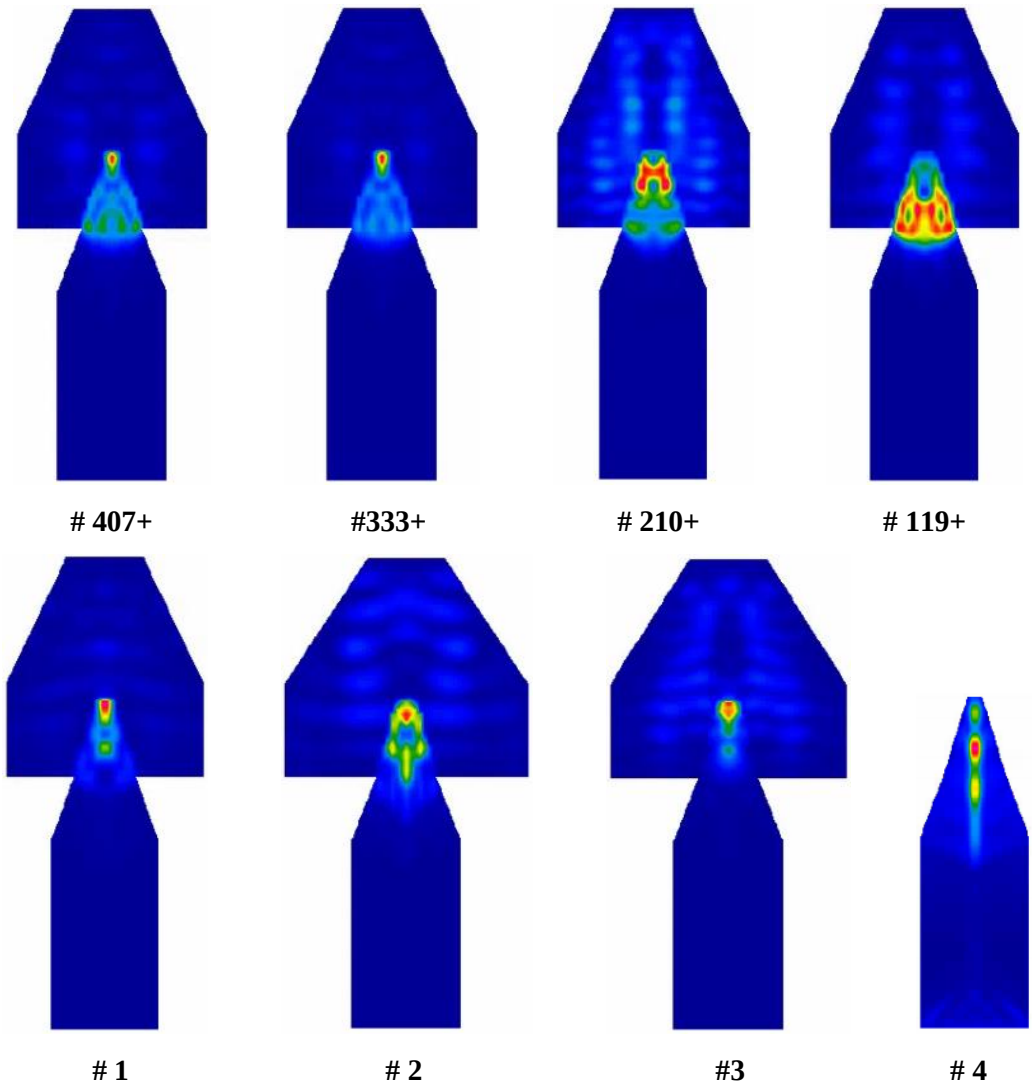

Figure 3.3 Selection of visualized dissipated power fields.

Table 3.4. Values of the Design Variables for the Patterns in Comparative Analysis

Pattern #	ε'	σ (S/m)	d_1	d_2	*RSD* (%)
1	56.9	0.669	67.5	55	60.7
2	62.9	0.136	62.8	55	80.3
3	49.3	0.154	78.1	55	135.6
4	0	0	0	0	111.5

The final results of the illustrative implementation of the optimization procedure are reported in Table 3.3. For comparison, in Table 3.4, we present four points corresponding to high RSD along with the related values of the design variables. Visualizations of the distribution of dissipated power for the optimized (first row) and non-optimized (second row) configurations of the dielectric insert are shown in Figure 3.3 (alternative representations of the presented patterns are included in Appendix A.2). In the first row, one can see distributions which are clearly more uniform within the region of interest than the ones in the second row. Distribution # 4 is particularly interesting because it shows the dissipated power in the animal's body and head without any dielectric insert. This can be taken as a direct parallel to the Gerling system outlined in Section 1.2. The RSD value in distribution # 4 is rated poorly at 111.5%; this illustrates that simply relying on the placement of the animal's head within the waveguide does not create the level of homogenous thermal treatment required for this application.

5. Conclusions

In this project, we have successfully created a fully parameterized model of the considered microwave fixation system that has been built for the full-wave 3D conformal FDTD electromagnetic simulator *QuickWave 2014*. An appropriate optimization problem has been formulated, and a corresponding optimization procedure has been developed and implemented in MATLAB environment. This procedure has been used to solve an illustrative optimization problem and determine the optimal characteristics of the dielectric insert. The output of this illustration has produced the parameters of the system in which the *RSD* was reduced from 120-135% (in non-optimized designs) to 23-27%. The achieved level appears to be the best for the chosen sub-space of the design variables, however, optimization in other sub-spaces (in particular with the dielectric constant being less than ε_m') may provide solutions with lower RSD. The optimization procedure appears to be suitable for homogenizing dissipated power in other microwave applicators with high rates of thermal processing.

Appendix

A. Mesh of the FDTD Model

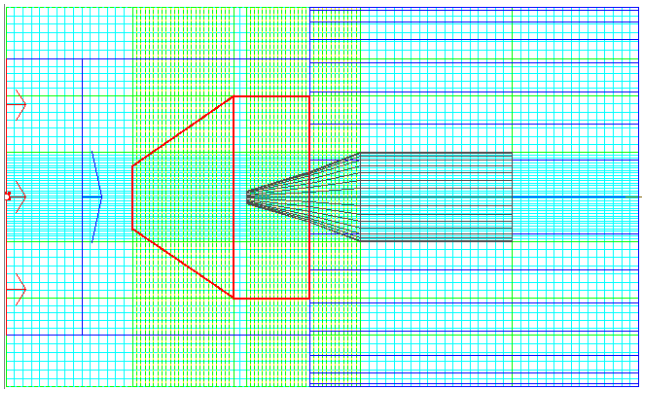

XZ-Plane

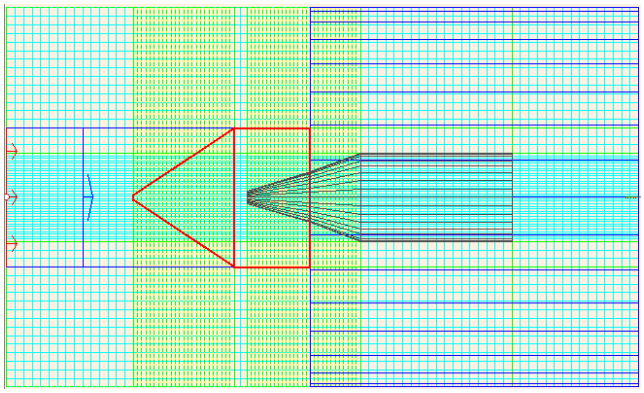

YZ-Plane

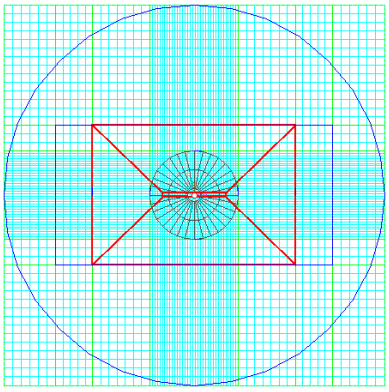

XY-Plane

B. Alternate Visualization of the Dissipated Power Fields (Figure 3.3)

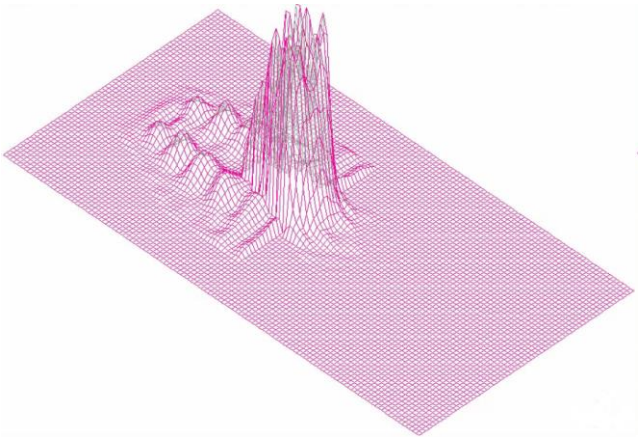

Pattern for Point 119+

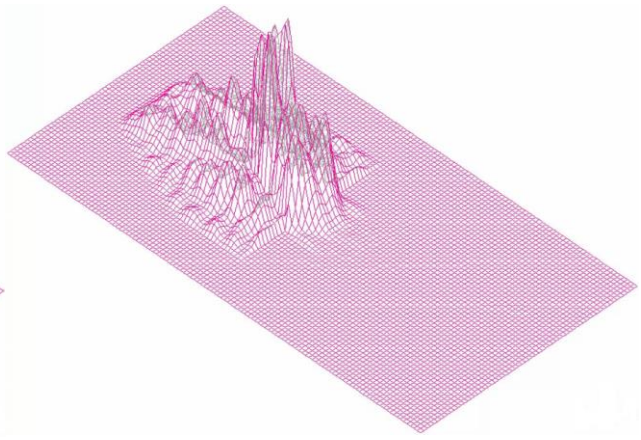

Pattern for Point 201+

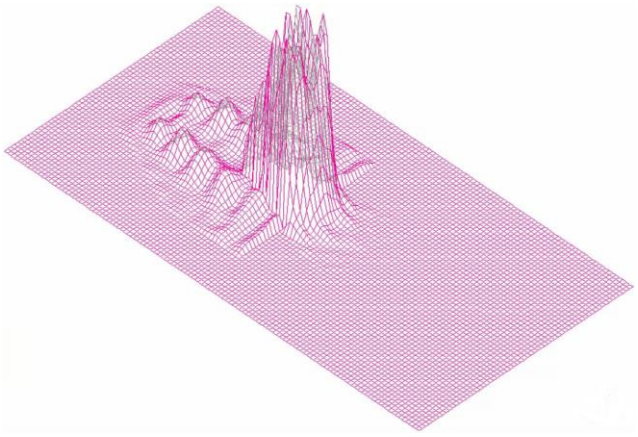

Pattern for Point 333+

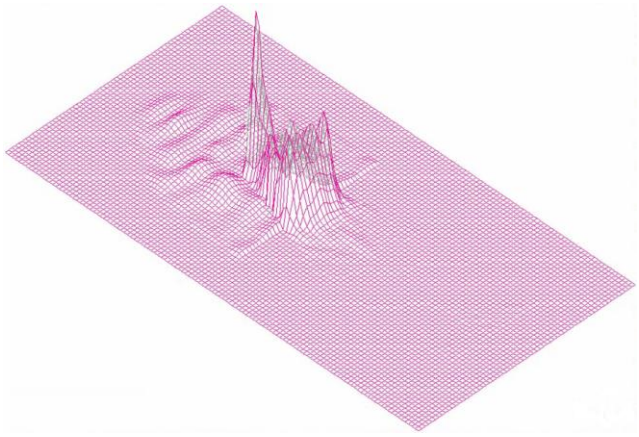

Pattern for Point 407+

C. *QuickWave 2014* UDO Script

```
comment="MQP 2015 MW Fixation System";
# bitmap="System1.bmp";

PAR( "Name ", oname, "System1");

# Rear cavity
PAR( "Diameter of cavity in xy-plane", drc, 150 );
PAR( "Height of cavity in z-dir.", hrc, 130 );

# Body's phantom
PAR( "Diameter of body's phantom in xy-plane", dbp, 35 );
PAR( "Height of body's phantom in z-dir.", hbp, 60 );

# Shoulder phantom
PAR( "Height of shoulder phantom", hsp, 20 );

# Head's phantom
PAR( "Base diameter of head's  phantom", bdhp, 20 );
PAR( "Top diameter of head's  phantom", tdhp, 5 );
PAR( "Height of head's  phantom", hhp, 25 );

# Waveguide
PAR( "Wavegude wide wall in x-dir.", a, 109 );
PAR( "Wavegude narrow wall in y-dir.", b, 55 );
PAR( "Wavegude length in z-dir.", w, 120 );

# Dielectric insert
PAR( "Diel. insert wide wall in x-dir.", da, 80 );
PAR( "Diel. insert narrow wall in y-dir.", db, 55 );
PAR( "Diel. insert length in z-dir.", dw, 30 );

# Dielectric pyramid
PAR( "Diel. pyramid length in z-dir.", dpw, 40 );
PAR( "Diel. pyramid top size in x-dir.", dptx, 25 );
PAR( "Diel. pyramid top size in y-dir.", dpty, 2 );

# Media
#PAR( "Diel. insert", diel, zirconia );
#PAR( "Animal", anim, brain);

# Mesh
PAR( "Cell size in air", cair, 5 );
PAR( "Cell size in animal", canim, 1.5 );
PAR( "Cell size in diel.insert",  cdiel, 3 );

#ports information
PAR("port IOP file",pname,pname);

ENDHEADER;

OPENOBJECT( oname );

OPENF(params.dat);
```

```
EPS1=READF;
EPS2=READF;
Sigma=READF;
da=READF;
db=READF;

MESHPAR ( cair, cair, cair, 1, 2, 1, 2, 1, 2, 1 );

INSERTMEDIUM("anim", ISOTROPIC) ;
MEDIUMPAR( anim, 46.9, 7.2, .98, 0, EPS1, 1, Sigma, 0, EPS1, 1, Sigma, 0, 0
);

# Rear cavity
CALL( "elements/cyv.udo", rearcavity, drc/2, hrc, 32, air, E, x, y, z, 10 );

# Body's phantom
CALL( "elements/cyv.udo", bphantom, dbp/2, hbp, 32, anim, E, x, y, z+hrc-
hbp-hsp, 10 );

# Shoulder phatom
CALL( "elements/tv.udo", shphantom, dbp/2, bdhp/2, hsp, 32, anim, E, x, y,
z+hrc-hsp, 11 );

# Waveguide
CALL( "elements/cubic.udo", wguide, a, b, w, air, x, y, z+hrc, 9 );


INSERTMEDIUM(dielTest, ISOTROPIC) ;
MEDIUMPAR( dielTest, EPS1, EPS2, Sigma, 0, EPS1, 1, Sigma, 0, EPS1, 1,
Sigma, 0, 0 );

# Dielectric insert
CALL( "elements/cubic.udo", dinsert, da, db, dw, dielTest, x, y, z+hrc, 9 );

# Dielectric pyramid
CALL( "elements/vtape.udo", dpyram, dpw, da, dptx, db, dpty, dielTest, E, x,
y, z+hrc+dw, 12 );

# Animal's head
CALL( "elements/tv.udo", ahead, bdhp/2, tdhp/2, hhp, 32, anim, E, x, y,
z+hrc, 11 );
# Port
CALL("elements/portz.udo", portname, a, b, DOWN, 1, 30, pname, x, y,
z+hrc+w, 11);

# SPs
# Insert and the body
CALL( "elements/specxu.udo", spxu1, 3, canim, x-da/2, y, z, 7 );
CALL( "elements/specxd.udo", spxd2, 3, canim, x+da/2, y, z, 7 );
CALL( "elements/specyu.udo", spyu1, 3, canim, x, y-db/2, z, 7 );
CALL( "elements/specyd.udo", spyd2, 3, canim, x, y+db/2, z, 7 );

CALL( "elements/speczu.udo", spzu1, 3, canim, x, y, z+hrc-hbp-hsp, 7 );
CALL( "elements/speczd.udo", spzd2, 3, canim, x, y, z+hrc+dw+dpw, 7 );

CLOSEOBJ;
```

References

[1] F. Mochel, and R.G. Haller, Energy deficit in huntington disease: why it matters, *J. of Clinical Investigation*, vol. 121, no. 2, pp. 493-99, 2011.

[2] Z. Chen, L.Y. Leung, A. Mountney, Z. Liao, W. Yang, X.C. Lu, J. Dave, Y. Deng-Bryant, G. Wei, K. Schmid, D.A. Shear, and F.C. Tortella, A novel animal model of closed-head concussive-induced mild traumatic brain injury: development, implementation, and characterization, *J. of Neurotrauma*, vol. 29, no. 2, pp. 268-80, 2012.

[3] K. Grundmann, N. Glöckle, G. Martella, G. Sciamanna, T.K. Hauser, L. Yu, S. Castaneda, B. Pichler, B. Fehrenbacher, M. Schaller, B. Nuscher, C. Haass, J. Hettich, Z. Yue, H.P. Nguyen, A. Pisani, O. Riess, and T. Ott, Generation of a novel rodent model for DYT1 dystonia, *Neurobiology of Disease*, vol. 47, no. 1, pp. 61-74, 2012.

[4] L.J Mcclay, D.E. Adkins, S.A. Vunck, A.M. Batman, R.E. Vann, S.L. Clark, P.M. Beardsley, and E. Oord, Large-scale neurochemical metabolomics analysis identifies multiple compounds associated with methamphetamine exposure, *Metabolomics*, vol. 9, no. 2, pp. 392-402, 2013.

[5] World Health Organization. Comprehensive Mental Health Action Plan 2013-2020. Geneva: World Health Organization, 2013, http://apps.who.int/gb/ebwha/pdf_files/WHA66/A66_R8-en.pdf.

[6] A.T. Modak, S.T. Weintraub, T.H. McCoy, and W.B. Stavinoha, Use of 300-msec microwave irradiation for enzyme inactivation: a study of effects of sodium pentobarbital on acetylcholine concentration in mouse brain regions, *J. of Pharmacology and Experimental Therapeutics*, vol. 197, no. 2, pp. 245-52, 1976.

[7] B.C. Cordes, E.E. Eves, and V.V. Yakovlev, Concept and technique of modeling-based homogenization of a temperature field in microwave heating systems, In: M. Celuch and V.V. Yakovlev, Eds., *Microwave Power Engineering with Advanced Computer Modeling*, CRC Press, 2015 (to be published).

[8] Muromachi Kikai Co., Ltd., Japan, http://www.muromachi.com.

[9] Gerling Applied Engineering, Inc., Modesto, CA, http://www.2450mhz.com.

[10] *QuickWave-3D*™, QWED Sp. z o. o., http://www.qwed.com.pl/.

[11] E.C. Burdette, F.L. Cain, and J. Seals, In vivo probe measurement technique for determining dielectric properties at VHF through microwave frequencies, *IEEE Trans. Microwave Theory and Tech.*, vol. 28, no. 4, pp. 414-427, 2003.